separations

MDPI

Article

Efficient Removal of Sr^{2+} by a Layered Metal Sulfide $K_{1.36}Cd_{1.12}Bi_{2.80}S_6$ via Ion Exchange

Lenian Qu [1,2,3], Yuxin Fang [1,3,4], Ziyi Wan [1,3,4], Meiling Feng [1,2,3,*] and Xiaoying Huang [1,2,3]

1 State Key Laboratory of Structural Chemistry, Fujian Institute of Research on the Structure of Matter, Chinese Academy of Sciences, Fuzhou 350002, China; qulenian@fjirsm.ac.cn (L.Q.); fangyuxin@fjirsm.ac.cn (Y.F.); wanziyi@fjirsm.ac.cn (Z.W.); xyhuang@fjirsm.ac.cn (X.H.)
2 University of Chinese Academy of Sciences, Beijing 100049, China
3 Fujian College, University of Chinese Academy of Sciences, Fuzhou 350002, China
4 College of Chemistry, Fuzhou University, Fuzhou 350116, China
* Correspondence: fml@fjirsm.ac.cn; Tel.: +86-591-63173146

Abstract

As a fission product of ^{235}U or ^{239}Pu, ^{90}Sr is a β-emitting radionuclide with a relatively long half-life ($t_{1/2}$ = 28.9 years). Due to its high solubility, easy environmental mobility, and propensity for bioaccumulation within the food chain, the development of efficient materials for the selective capture of $^{90}Sr^{2+}$ is critical for the safe disposal of nuclear waste and environmental protection. In this study, a layered metal sulfide, $K_{1.36}Cd_{1.12}Bi_{2.80}S_6$ (denoted as KCBS), was synthesized via the high-temperature solid-phase method using K_2CO_3 as the potassium source. KCBS demonstrates high adsorption performance towards Sr^{2+}, achieving a maximum adsorption capacity (q_m^{Sr} = 77 mg·g^{-1}). Moreover, it can maintain high adsorption efficiency (R^{Sr} > 84.15%) across a broad pH range of 2.98–12.01. In addition, KCBS exhibits the outstanding selectivity for Sr^{2+} removal in the presence of excessive Na^+ ions and even in actual water samples. KCBS also possesses regenerability, maintaining its superior adsorption capacity for Sr^{2+} ions over three cycles. The mechanism study by energy-dispersive X-ray spectroscopy (EDS) and X-ray photoelectron spectroscopy (XPS) analyses indicates that the efficient Sr^{2+} capture is attributed to the ion exchange between Sr^{2+} and interlayer K^+ ions in KCBS. This research further highlights the potential of layered metal sulfide ion exchange materials for radionuclide remediation.

Keywords: strontium; metal sulfide; ion exchange; adsorption capacity; selectivity

1. Introduction

Nuclear energy plays a pivotal role in the global energy transition due to its high efficiency, stability, and low-carbon characteristics. However, the nuclear fuel cycle inevitably generates substantial volumes of radioactive liquid waste, for which its safe and long-term disposal is critical to the sustainable development of nuclear energy [1–3]. Strontium-90 (^{90}Sr), as a primary fission product of ^{235}U and ^{239}Pu, is one of the major radioactive sources in high-level radioactive liquid wastes [4,5]. ^{90}Sr is characterized by a long half-life ($t_{1/2}$ = 28.79 years), strong radioactivity (emitting high-energy β rays), and high heat release [6]. Notably, ^{90}Sr typically exists in the environment as $^{90}Sr^{2+}$ ions with high water solubility and mobility [7]. Due to its similar chemical properties with respect to Ca^{2+} ions, $^{90}Sr^{2+}$ can easily enter organisms through the food chain and accumulates in bones, constituting a persistent radiation risk [8]. In radioactive liquid waste, $^{90}Sr^{2+}$ frequently coexists with interfering ions such as Na^+, Mg^{2+}, and Ca^{2+} [9,10]. This poses a significant challenge

Check for updates

Academic Editor: Hao Li

Received: 10 January 2026
Revised: 14 February 2026
Accepted: 15 February 2026
Published: 18 February 2026

Copyright: © 2026 by the authors. Licensee MDPI, Basel, Switzerland. This article is an open access article distributed under the terms and conditions of the Creative Commons Attribution (CC BY) license.

for the selective removal of Sr^{2+} ions. In addition, ^{90}Sr serves as a β radiation source with applications in the field of industrial [11] and radiological medicine [12]. Consequently, the highly efficient removal and recovery of $^{90}Sr^{2+}$ from complex radioactive liquid wastes are of vital importance for the sustainable development of nuclear energy, ecological and environmental safety, and resource utilization.

Currently, various methods have been explored to remove Sr^{2+} from radioactive liquid wastes, primarily including solvent extraction, chemical precipitation, membrane filtration, and adsorption/ion exchange [13]. Among these, ion exchange is considered a more ideal treatment method due to its operational simplicity, high efficiency, and minimal secondary pollution generation [14,15]. Among the various ion exchange materials used for Sr^{2+} removal, organic ion exchange resins are widely applied. However, they face problems of high cost and long-term stability [16]. By contrast, inorganic ion exchange materials (such as titanates [17,18], clays [19], and zeolites [20]) offer significant advantages due to their outstanding chemical stability and easy post-treatment [21]. However, current inorganic ion exchangers still face some application limitations, including narrow pH ranges, limited adsorption capacity, and poor selectivity for Sr^{2+} [22,23].

In recent years, metal sulfide ion exchangers (MSIEs) have shown promising prospects in the field of radioactive contamination remediation [15,24–26]. MSIEs can remove Sr^{2+} ions through the ion exchange of Sr^{2+} with charge-balanced cations within interlayer spaces or channels of the anionic framework of MSIEs. S^{2-} in the anionic framework of MSIEs serves as Lewis soft base sites that are easily polarized, inducing metal–sulfur bond distortion and conferring structural flexibility, which results in the breathing effect and adaptive modulation of interlayer or channel spacing to facilitate Sr^{2+} entry and the ion exchange process [16]. To date, MSIEs for Sr^{2+} removal mainly are Sn-containing metal sulfides, such as the KMS series (e.g., $K_{2x}Mg_xSn_{3-x}S_6$, q_m^{Sr} = 86.89 mg·g^{-1} [27]), KTS series (e.g., $K_{2x}Sn_{4-x}S_{8-x}$, q_m^{Sr} = 102 mg·g^{-1} [28]) and its derivatives (e.g., $Na_2Sn_3S_7$, q_m^{Sr} = 80 mg·g^{-1} [29] and $Na_{1.94}Sn_{2.87}S_7$, q_m^{Sr} = 88.9 mg·g^{-1} [30]), FJSM-SnS series (e.g., $(Me_2NH_2)_{1.33}(Me_3NH)_{0.66}Sn_3S_7$, q_m^{Sr} = 65.19 mg·g^{-1} [31] and $[CH_3NH_3][Bmmim]Sn_3S_7$, q_m^{Sr} = 59.41 mg·g^{-1} [32]), and FJSM-KSnS ($K_2Sn_2S_5$, q_m^{Sr} = 59.88 mg·g^{-1} [33]). However, research on Sn-free MSIEs for Sr^{2+} removal remains quite limited. Only a few examples, such as InS-1 ($[CH_3CH_2NH_3]_6In_6S_{12}$, q_m^{Sr} = 105.35 mg·g^{-1} [34]), K-TaS_2 ($K_{0.33}TaS_2$, q_m^{Sr} = 37.95 mg·g^{-1}), and K-TbS_2 ($K_{0.36}NbS_2$, q_m^{Sr} = 79.25 mg·g^{-1}), have been reported [35]. In addition, the adsorption capacity and selectivity for Sr^{2+} capture by MSIEs are still unsatisfactory. Therefore, new MSIEs still require development for Sr^{2+} removal.

Herein, a layered metal sulfide $K_{1.36}Cd_{1.12}Bi_{2.80}S_6$ (denoted as KCBS) was prepared via the high-temperature solid-phase method using K_2CO_3 as the potassium source. KCBS exhibits a Bi_2Se_3-type structure, consisting of anionic layers of $[Cd_{1.12}Bi_{2.80}S_6]_n^{1.36n-}$ and exchangeable K^+ ions in the interlayer spaces. KCBS shows high adsorption capacity (q_m = 77 mg·g^{-1}) and rapid kinetic response (t = 30 min, R^{Sr} = 95.08%) for Sr^{2+} removal. It maintains high Sr^{2+} removal efficiency (R^{Sr} > 84.15%) in the pH range from 2.98 to 12.01, while preserving framework stability and achieving low Cd and Bi leaching rates (R_L < 0.02%). Notably, KCBS can effectively remove Sr^{2+} in the presence of excessive Na^+ ions and various competing ions, as well as in actual water samples. Furthermore, adsorption and desorption experiments demonstrate that KCBS can be readily regenerated using 2 mol·L^{-1} KCl solution as the eluent and maintain framework stability and Sr^{2+} removal efficiency after three regeneration cycles. Characterizations, including energy-dispersive X-ray spectroscopy (EDS), X-ray photoelectron spectroscopy (XPS), and powder X-ray diffraction (PXRD), reveal that the efficient Sr^{2+} removal is attributed to the ion exchange between Sr^{2+} and interlayer K^+. This work provides a new metal sulfide scavenger

for Sr^{2+} with high removal performance and highlights the development of metal sulfide ion exchange materials for radioactive contamination remediation.

2. Materials and Methods

2.1. Materials

S (99.50%), NaCl (AR), $MgCl_2 \cdot 6H_2O$ (AR), and HNO_3 (69%) were purchased from Sinopharm Chemical Reagent Co., Ltd. (Shanghai, China). KCl (AR) was purchased from Tianjin Fengchuan Chemical Reagent Co., Ltd. (Tianjin, China). Bi_2S_3 (99.999%) was obtained from Adamas Reagent Co., Ltd. (Shanghai, China). Cd (AR) was purchased from Tianjin Jinke Fine Chemical Industry Research Institute Co., Ltd. (Tianjin, China). $CaCl_2 \cdot 2H_2O$ (74%) was purchased from Shanghai Sili Chemical Plant (Shanghai, China). CsCl (99.99%) was purchased from Shanghai Longjin Metallic Material Co., Ltd. (Shanghai, China). $SrCl_2 \cdot 6H_2O$ (AR) and NaOH (AR) were obtained from Guangfu Fine Chemical Research Institute (Tianjin, China). All reagents were used directly after purchase without undergoing any processing.

2.2. Methods

2.2.1. Synthesis of $K_{1.36}Cd_{1.12}Bi_{2.80}S_6$ (KCBS)

The crystalline samples of KCBS were synthesized via solid-state reaction. Previously, K_2S_2 was employed as the potassium source for the preparation of $K_{1.83}Cd_{1.83}Bi_{2.17}S_6$ [36], a compound with a similar layered structure to that of KCBS. However, alkali metal polysulfides like K_2S_2 are susceptible to degradation upon air exposure, making them unsuitable for long-term storage unless kept inside a glove box. Furthermore, alkali metal polysulfides are commonly synthesized using liquid ammonia, posing operational risks [37,38]. To avoid these issues, K_2CO_3 was used instead of K_2S_2 as the potassium source in this study, and a pure phase of KCBS was successfully obtained under simple synthesis conditions. The synthesis procedure is as follows. A mixture of K_2CO_3 (0.45 mmol, 0.0622 g), Bi_2S_3 (0.5 mmol, 0.2571 g), Cd (0.4 mmol, 0.045 g), and S (1 mmol, 0.032 g) was thoroughly ground. The resultant powder mixture was loaded into a quartz tube (outer diameter of 12 mm, inner diameter of 10 mm, and length of 30 cm). The quartz tube was evacuated to a pressure below 100 Pa and then sealed, which underwent thermal treatment in a muffle furnace according to the following program: heating from room temperature to 350 °C within 12 h and holding at 350 °C for 12 h and then heating to 780 °C within 12 h and holding at 780 °C for 16 h and finally slowly cooling to 300 °C within 96 h, followed by natural cooling to room temperature. Subsequently, the solid product was repeatedly washed with deionised water and ethanol. During the washing process, a loss of the supernatant black fine microcrystals occurred. Then, the black plate-like crystals were collected (yield: 0.252 g, 74% based on Cd).

2.2.2. Characterization Techniques

Powder X-ray diffraction (PXRD) measurements were performed on a Rigaku Miniflex II diffractometer (Japan) using Cu$K\alpha$ radiation (λ = 1.54178 Å) at 30 kV and 15 mA, with data collected across a 2θ range spanning 5° to 65°. Single-crystal X-ray diffraction data were acquired on a Rigaku diffractometer (Japan) utilizing graphite-monochromated Mo$K\alpha$ radiation (λ = 0.71073 Å). X-ray photoelectron spectroscopy (XPS) measurements were conducted on an ESCALAB 250Xi spectrometer (Thermo Scientific, Waltham, MA, USA) using Al$K\alpha$ radiation. Thermogravimetric analysis (TGA) was carried out on a NETZSCH STA 449 F3 instrument (Netzsch, Germany) under a nitrogen atmosphere at a heating rate of 10 °C·min^{-1}. Morphological and elemental analyses were performed using a field-emission scanning electron microscope (FE-SEM, JSM-6700F, JEOL, Akishima, Tokyo,

Japan) equipped with energy-dispersive X-ray spectroscopy (EDS) for elemental mapping. Elemental concentrations were determined by inductively coupled plasma mass spectrometry, including tandem mass spectrometry (ICP-MS/MS, Agilent 8900, Santa Clara, CA, USA) and conventional ICP-MS (Thermo XSeries II, Waltham, MA, USA), following stringent quality assurance protocols such as the use of calibration standards and repeated measurements.

2.2.3. Batch Adsorption Experiments

Ion Exchange Experiment: In a typical procedure, a measured amount of KCBS crystals was mixed with a Sr^{2+}-containing solution at a solid-to-liquid ratio of 1000 mL·g^{-1}. Unless otherwise specified, all exchange experiments were conducted at room temperature in a shaking incubator operating at 160 rpm. After reaction, the supernatant was collected by natural settling followed by filtration through a 0.22 μm membrane, diluted with 2% HNO_3, and analyzed for residual Sr^{2+} concentration using ICP-MS/MS and ICP-MS. Solid samples were washed sequentially with deionized water and ethanol, air-dried at room temperature, and stored for subsequent characterization (PXRD, EDS, TG, etc.).

Isothermal Adsorption Experiment: In total, 10 mg of KCBS crystal samples was mixed with 10 mL of Sr^{2+} solutions with varying initial concentrations (C_0^{Sr}: 3.31 to 537 mg·L^{-1}). The mixture was shaken for 12 h. The adsorption data were fitted to the Langmuir, Freundlich, and Langmuir–Freundlich models for the calculation of the maximum adsorption capacity.

Adsorption Kinetics Experiment: In total, 50 mg of KCBS was added to 50 mL of Sr^{2+} solution (C_0^{Sr} = 6.45 mg·L^{-1}) and stirred magnetically. Aliquots (~1 mL) were taken at specific time intervals. After separation, the residual Sr^{2+} concentrations were measured. The kinetic data were analyzed employing pseudo-first-order and pseudo-second-order kinetic models.

Adsorption Thermodynamic Experiment: Experiments were carried out at 293, 313, and 333 K, with 10 mg of KCBS added to 10 mL of a Sr^{2+} solution (C_0^{Sr} = 10.58 mg·L^{-1}), which was magnetically stirred throughout the process.

Acid–Base Stability Experiment: Sr^{2+}-containing solutions with different pH values ranging from 1 to 12 (C_0^{Sr}: 3.49–5.30 mg·L^{-1}) were prepared using nitric acid solution or sodium hydroxide solution. Then, 10 mg of KCBS was mixed with 10 mL of the above solutions and shaken for 12 h. The solid residues were washed with deionised water and ethanol and characterized by PXRD.

Competitive Experiment: Solutions with various molar ratios (M/Sr^{2+}) were prepared (M = Cs^+, Na^+, Mg^{2+}, or Ca^{2+}). Mixed solutions containing multiple ions were also prepared. In addition, Sr^{2+} was spiked into various water samples, including tap water (Fuzhou, China), lake water (Qishan Lake, Fuzhou, China), river water (Wulong River, Fuzhou, China), and seawater (Dongshan Island, Zhangzhou, China), to simulate polluted water environments.

Adsorption Experiment after Irradiation: In total, 10 mg samples of KCBS irradiated with β and γ rays at doses of 100 kGy and 200 kGy were placed in 10 mL of Sr^{2+} solution (C_0^{Sr} = 8.07 mg·L^{-1}) for an adsorption study.

Adsorption and Desorption Experiment: In total, 250 mg of KCBS was added to 250 mL of 1000 mg·L^{-1} Sr^{2+} solution and shaken for 12 h. The products after adsorption were washed with deionized water and ethanol, dried, and then characterized by EDS, Element Mapping, and PXRD. Then, the product was immersed in a 2 mol·L^{-1} KCl solution at a solid-to-liquid ratio of 1000 mL·g^{-1} and shaken for 12 h to desorb Sr^{2+}. The desorbed sample was similarly washed with deionized water and ethanol, dried, and characterized. Finally, the adsorption and regenerative capacity were evaluated using the Sr^{2+} solution

(C_0^{Sr} = 7.9 mg·L^{-1}) and 2 mol·L^{-1} KCl solution. The adsorption–desorption–re-adsorption cycle was repeated three times to assess cycling stability.

3. Results

3.1. Crystal Structure and Characterization

Single-crystal X-ray analysis reveals that KCBS crystallizes in the space group $P6_3/mmc$ (Tables S1–S3). Its structure features a two-dimensional anionic layer of $[Cd_{1.12}Bi_{2.80}S_6]_n^{1.36n-}$ with K^+ ions located in the interlayer spaces. [(Bi/Cd)S_6] octahedra form the Bi_2Se_3-type anionic layers of $[Cd_{1.12}Bi_{2.80}S_6]_n^{1.36n-}$ (Figure 1a) by edge-sharing. Different from the previously reported $K_{1.83}Cd_{1.83}Bi_{2.17}S_6$ with only two crystallographically independent potassium sites (K1, K2) in the asymmetric unit, there are three crystallographically independent potassium sites (K1, K2, K3) in $K_{1.36}Cd_{1.12}Bi_{2.80}S_6$ (KCBS) (Table S4) [36]. In addition, compared with the anionic layers of $[Cd_{1.83}Bi_{2.17}S_6]_n^{1.83n-}$ in $K_{1.83}Cd_{1.83}Bi_{2.17}S_6$, the anionic $[Cd_{1.12}Bi_{2.80}S_6]_n^{1.36n-}$ layers in KCBS contain more Cd vacancies, resulting in a slightly higher K/Cd ratio. These structural differences are likely attributable to the distinct synthesis conditions. Previous research has demonstrated that the ion exchange performance of two-dimensional MSIEs exhibits an inverted U-curve rule with the interlayer $d_{S\text{-}S}$ [35]. Specifically, when the $d_{S\text{-}S}$ of MSIEs falls within the range of 4.676 to 6.403 Å, they may exhibit good ion exchange performance. The interlayer $d_{S\text{-}S}$ in KCBS is 5.201 Å, which suggests that the current compound possesses significant ion exchange potential (Figure 1b).

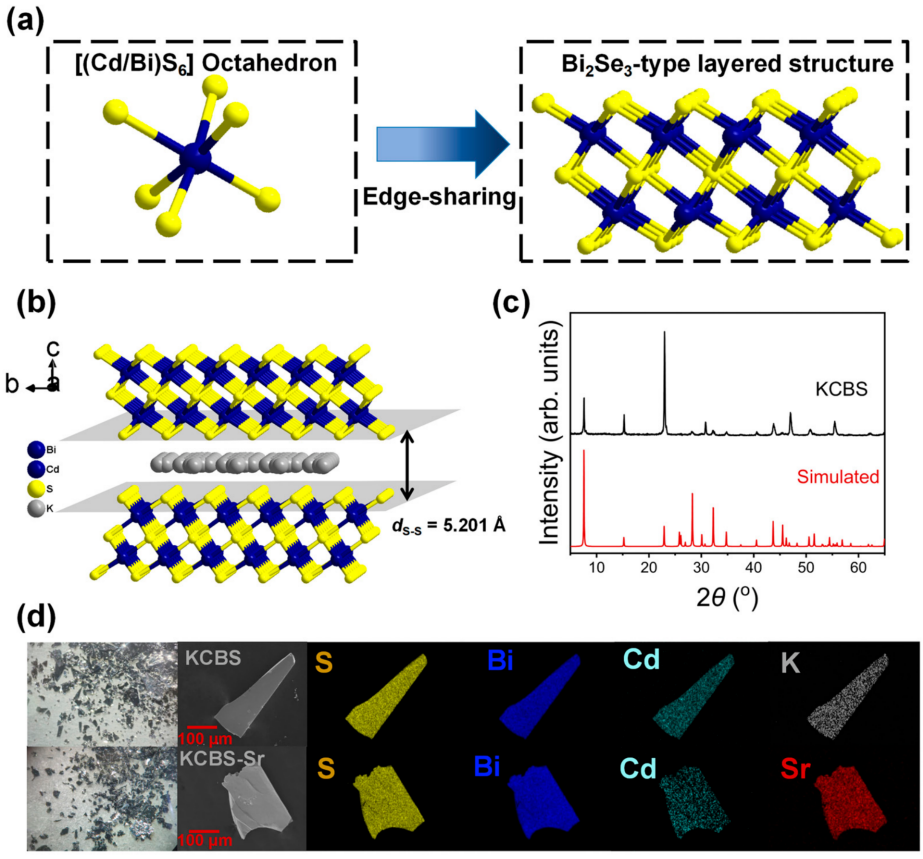


Figure 1. (**a**) Schematic of [(Cd/Bi)S_6] octahedron and a Bi_2Se_3-type anionic layer of $[Cd_{1.12}Bi_{2.80}S_6]_n^{1.36n-}$. (**b**) Packing diagram of KCBS viewed along the a-axis, showing the layers stacking and interlayer disordered K^+ ions, with the interlayer d_{s-s} indicated. (**c**) Experimental and simulated PXRD patterns of KCBS. (**d**) Photographs of KCBS and KCBS-Sr crystal samples, along with corresponding SEM images and elemental distribution maps.

The PXRD pattern of KCBS exhibits agreement with the simulated pattern from the single-crystal X-ray structure, confirming a pure phase (Figure 1c). The discrepancy in the intensity of some diffraction peaks is likely due to the preferred orientation. In total, 100 mg of KCBS crystal samples was immersed in 100 mL of a 1000 mg·L^{-1} Sr^{2+} solution and shaken at room temperature for 12 h. The obtained adsorption product is denoted as KCBS-Sr. Elemental distribution maps (Figure 1d) and EDS (Figure S1a,b) results confirm the successful replacement of K^+ by Sr^{2+}. The surface morphology of the material, as observed by scanning electron microscopy (SEM), shows no significant change upon substitution of K^+ with Sr^{2+} (Figure S2). The TGA curve reveals that KCBS exhibits approximately 2% mass loss between 25 °C and 125 °C (Figure S1c), which is attributed to the loss of adsorbed surface water. No significant mass change occurs between 125 °C and 700 °C, indicating the high thermal stability of KCBS. Meanwhile, KCBS-Sr exhibits a mass loss of approximately 7.3% from 20 to 500 °C, primarily attributable to the desorption of water molecules from the hydrated Sr^{2+} ions in it.

3.2. Adsorption Isotherm and Adsorption Kinetics Studies

The maximum adsorption capacity of KCBS for Sr^{2+} was investigated through systematic adsorption isotherm experiments. The relationship between Sr^{2+} adsorption amount (q_e^{Sr}, Equation (S1)) and equilibrium concentration (C_e^{Sr}) is illustrated (Figure 2a and Table S5). The isotherm data are fitted using the Langmuir (Equation (S2)), Freundlich (Equation (S3)), and Langmuir–Freundlich models (Equation (S4)) [39]. Among them, the Langmuir–Freundlich model exhibits the highest goodness-of-fit (R^2 = 0.98396), outperforming both the Langmuir model (R^2 = 0.97557) and the Freundlich model (R^2 = 0.96663) (Table S6). Calculations based on the Langmuir–Freundlich model indicate that the maximum adsorption capacity of KCBS for Sr^{2+} (q_m^{Sr}) is 77 mg·g^{-1}, which exceeds that of some reported Sr^{2+} adsorbents, such as $Na_5Zn_{3.5}Sn_{3.5}S_{13}$ (32.3 mg·g^{-1}) [40], $Na_{1.60}Mg_{0.33}Sn_{3.15}S_7$ (52.6 mg·g^{-1}) [41], and $(Me_2NH_2)_{1.33}(Me_3NH)_{0.66}Sn_3S_7$ (65.19 mg·g^{-1}) [31], as well as SnO_2-Sb_2O_5 (25.7 mg·g^{-1}) [42] and AMP-PAN (16 mg·g^{-1}) [43] (Table S7).

Furthermore, the Sr^{2+} adsorption kinetics of KCBS were investigated. The Sr^{2+} concentration rapidly decreases from 6.45 mg·L^{-1} to 1.77 mg·L^{-1} within 15 min, achieving a high removal efficiency (R^{Sr}, Equation (S5)) of approximately 95.08% at 30 min (Figure 2b and Table S8), which indicates a rapid and highly efficient adsorption process. The kinetic data are successfully fitted to both the pseudo-first-order and pseudo-second-order models (Equations (S6) and (S7), Figure S3 and Table S9).

3.3. Adsorption Thermodynamics Study

The thermodynamic behavior of KCBS for Sr^{2+} adsorption was investigated within the temperature range of 293 K to 333 K. The results indicate that the distribution coefficient (K_d^{Sr}, Equation (S8)) increases progressively with rising temperatures, suggesting that higher temperatures are more favorable for the adsorption process (Figure 2c and Table S10). Concurrently, relevant thermodynamic parameters are calculated based on thermodynamic models (Equations (S9)–(S11)). Both the enthalpy change (ΔH^0) and entropy change (ΔS^0) are positive values (ΔH^0 = 56.52 kJ·mol^{-1}, ΔS^0 = 0.27 kJ·mol^{-1}·K^{-1}). Therefore, all measured Gibbs free energy changes (ΔG^0) are negative, confirming the spontaneity of this adsorption process. As the temperature increases from 293 K to 333 K, ΔG^0 decreases gradually from −22.49 kJ·mol^{-1} to −33.28 kJ·mol^{-1}, further indicating that higher temperatures are of benefit to Sr^{2+} adsorption.

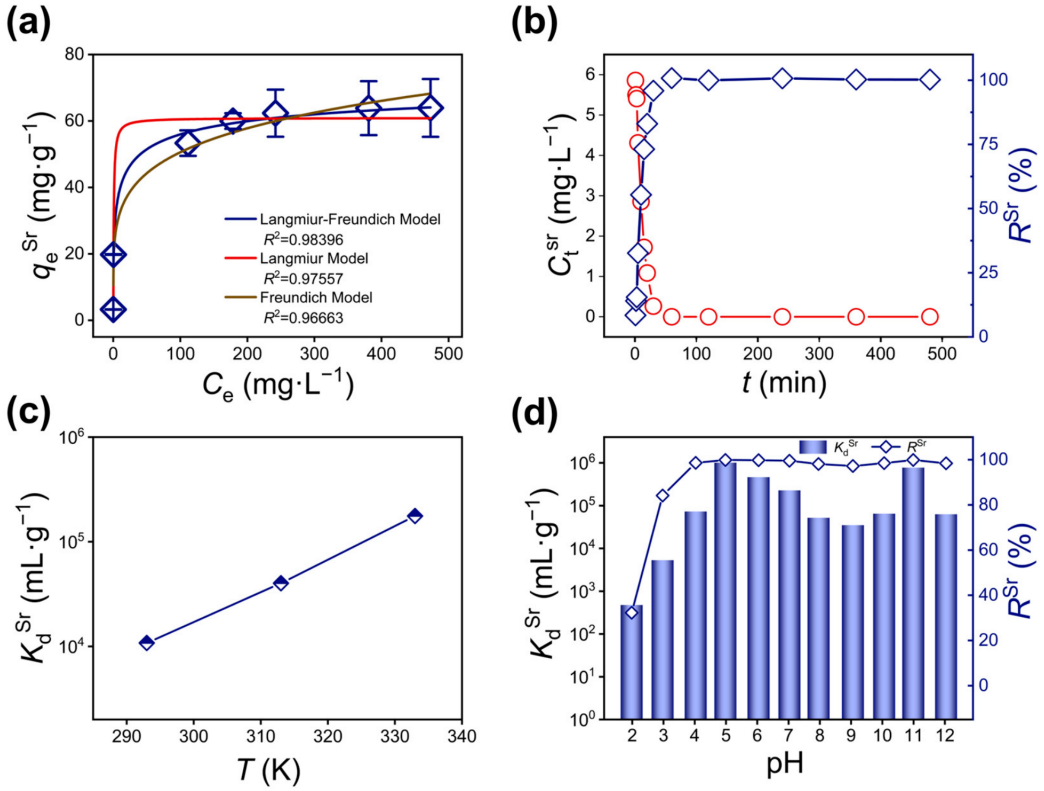


Figure 2. (**a**) Adsorption isotherms of KCBS for Sr^{2+} fitted using the Langmuir, Freundlich, and Langmuir–Freundlich models. (**b**) Kinetic curves of KCBS plotted with $C_t{}^{Sr}$ (red line) and R^{Sr} (blue line) vs. time t (min). (**c**) Effect of temperature on Sr^{2+} adsorption by KCBS. (**d**) $K_d{}^{Sr}$ (mL·g^{-1}) (column) and R^{Sr} (%) (dotted line plot) values of KCBS at different pH values.

3.4. Effect of pH on Sr^{2+} Adsorption

Considering the variable acidity and alkalinity of nuclear wastewater, solution pH critically affects the removal efficiency of radioactive nuclides. The adsorption performance of KCBS towards Sr^{2+} was systematically evaluated across a pH range of 2.01 to 12.01. The results show that KCBS maintains high R^{Sr} above 84.15% within a broad pH range of 2.98 to 12.01 (Figure 2d). Even under strongly acidic conditions (pH = 2.01), the R^{Sr} is 32.26%. Under strongly alkaline conditions (pH = 12.01), KCBS still exhibits good adsorption performance with an R^{Sr} of 98.42%, and the $K_d{}^{Sr}$ reaches 6.27×10^4 mL·g^{-1}. Furthermore, Cd and Bi leaching rates (R_L, Equation (S12)) in solutions after adsorption are below 0.02% throughout the pH range of 2.01 to 12.01, indicating excellent material stability (Figure S4b and Table S11). PXRD analyses confirm that the layered framework of KCBS remains intact after adsorption under various pH values (Figure S4a). KCBS shows outstanding and stable Sr^{2+} removal capability over a wide pH range from acidic to strongly alkaline, making it a promising candidate for treating nuclear wastewater with complex pH conditions.

3.5. Effect of Competitive Metal Ions

Nuclear wastewater contains substantial amounts of competitive ions such as Na^+, Cs^+, Ca^{2+}, and Mg^{2+}, for which their presence may significantly affect the removal of Sr^{2+}. Therefore, the adsorption capacity of KCBS towards Sr^{2+} in the presence of competitive metal ions was systematically investigated. At different Na/Sr molar ratios from 7.03 to 131.35, $K_d{}^{Sr}$ consistently remained above 10^4 mL·g^{-1}, and R^{Sr} exceeded 92.2% (Figure 3a and Table S12). Notably, at a Na/Sr molar ratio of 7.03, the separation factor ($SF_{Sr/Na}$, Equation (S13)) of KCBS reaches 3789.77. These results demonstrate that KCBS can efficiently and selectively separate Sr^{2+} under high concentrations of Na^+. Furthermore,

the selective removal of Sr^{2+} was investigated under coexisting Cs^+ and Na^+. When the Sr/Cs/Na molar ratio is 1:2.32:72.30, R^{Sr} still reaches 89.95%. Even when the Sr/Cs/Na molar ratio increases to 1:4.69:137.94, R^{Sr} remains at 63.7% (Figure S5 and Table S13). This indicates that KCBS retains Sr^{2+} removal capacity in the presence of mixed monovalent alkali metal ions.

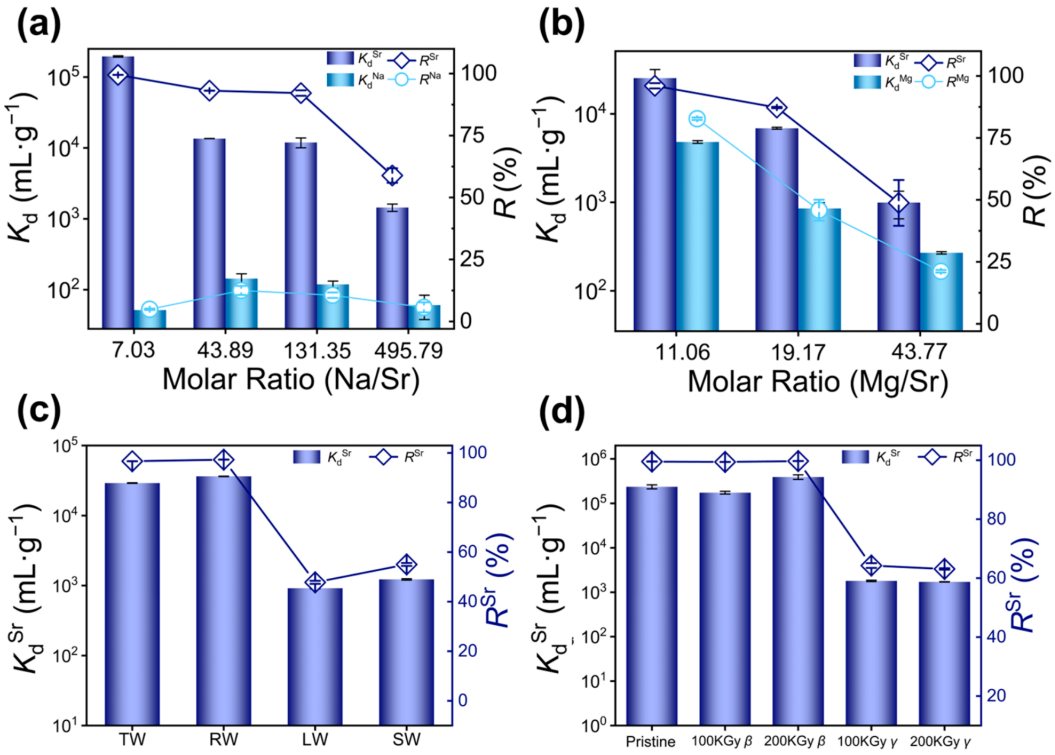


Figure 3. (**a**) K_d (mL·g^{-1}) (column) and R (%) (dotted line plot) of KCBS for Sr^{2+} and Na^+ removal in solutions with different Na/Sr molar ratios. (**b**) K_d (mL·g^{-1}) (column) and R (%) (dotted line plot) of KCBS for Sr^{2+} and Mg^{2+} removal in solutions with different Mg/Sr molar ratios. (**c**) K_d^{Sr} (mL·g^{-1}) (column) and R(%) (dotted line plot) of KCBS for Sr^{2+} removal in tap water (TW), river water (RW), lake water (LW), and sea water (SW). (**d**) K_d^{Sr} (mL·g^{-1}) and R^{Sr} (%) (dotted line plot) of KCBS samples before and after 100/200 kGy β/γ irradiation.

Competitive adsorption experiments were also carried out to assess the interference of divalent ions Ca^{2+} and Mg^{2+} on Sr^{2+} removal by KCBS. When the Mg/Sr molar ratios range from 11.06 to 19.17, K_d^{Sr} remains above 10^3 mL·g^{-1}, with R^{Sr} exceeding 87.3%. Increasing the Mg/Sr ratio to 43.77 leads to a significant decline in K_d^{Sr} to 993 mL·g^{-1} and R^{Sr} to 49% (Figure 3b, Table S14). When the Ca/Sr ratio is 3.54, K_d^{Sr} surpasses 10^4 mL·g$^{-1,}$ and R^{Sr} reaches 98.82%. Once the ratio exceeds 5.64, however, K_d^{Sr} drops below 10^3 mL·g^{-1}, and R^{Sr} is lower than 56.6% (Figure S6 and Table S15). These results confirm that KCBS effectively removes Sr^{2+} in the presence of low concentrations of Mg^{2+} or Ca^{2+}. Even within the complex system featuring molar ratios of Sr/Na/Cs/Mg/Ca at 1:75.82:2.27:6.97:3.16, the R^{Sr} of KCBS is 67.0% (Table S16). However, the above results indicate that the presence of high-concentration Mg^{2+} and Ca^{2+} significantly affects the removal efficiency of Sr^{2+}.

To simulate the actual Sr^{2+} removal efficiency in actual environmental water samples, low-concentration Sr^{2+} (C_0^{Sr}: 3.028–3.43 mg·L^{-1}) was artificially added to tap water, river water, lake water, and sea water to evaluate the adsorption performance of KCBS for Sr^{2+}. The results demonstrate that KCBS exhibits outstanding Sr^{2+} adsorption performance in tap water and river water, with K_d^{Sr} being more than 10^4 mL·g^{-1} and R^{Sr} being higher than 96.68% (Figure 3c and Table S17). In lake water and seawater, K_d^{Sr} values are 916 mL·g^{-1} and 1.22 × 10^3 mL·g^{-1}, respectively, with corresponding R^{Sr} values of 47.8% and 55.0%.

3.6. Study on the Irradiation Stability of KCBS

In the process of treating radioactive wastewater, adsorbents are often subjected to high levels of radiation, which can damage their structural integrity and reduce their capacity to remove target radionuclides. Consequently, the Sr^{2+} adsorption performance of KCBS was investigated using samples before and after irradiation with 100/200 kGy β-rays and 100/200 kGy γ-rays. By comparing the PXRD patterns of the original and irradiated samples, it is confirmed that KCBS can maintain structural stability after strong irradiation, exhibiting no obvious collapse or transformation (Figure S7). Furthermore, the $K_d{}^{Sr}$ of KCBS after β irradiation exceeds 10^5 mL/g, with R^{Sr} exceeding 99.43%. By contrast, KCBS samples subjected to 100 and 200 kGy γ irradiation exhibit $K_d{}^{Sr}$ at the level of 10^3 mL·g^{-1}, with a corresponding R^{Sr} of 64.3% and 63.1%, respectively (Figure 3d and Table S18). This indicates that β irradiation does not affect the Sr^{2+} removal capacity of KCBS, whereas γ irradiation causes a decline in the Sr^{2+} adsorption performance of KCBS.

3.7. Adsorption and Desorption

To investigate the regeneration performance of KCBS-Sr, adsorption–desorption cycling experiments were conducted. Initially, the desorption efficiency of Sr^{2+} from KCBS-Sr was explored using a 2 mol·L^{-1} KCl solution as the eluent. The 2 mol·L^{-1} KCl solution can effectively desorb Sr^{2+} from KCBS-Sr, yielding the product noted as KCBS-Sr-K (Figures 4a and S8b). The PXRD patterns show that the layered framework of the current metal sulfide remains stable throughout this process (Figure S8a). Accordingly, removal and desorption efficiencies are systematically studied across three adsorption cycles. R^{Sr} remains consistently above 99.94% throughout the three cycles, with desorption efficiency (E^{Sr}, Equation (S14)) approaching 100% (Figure 4c and Table S19). Furthermore, PXRD patterns reveal that samples maintain their layered structure after each adsorption and regeneration cycle, showing no signs of collapse (Figure 4b). Consequently, KCBS enables simple and efficient regeneration using the 2 mol·L^{-1} KCl solution while preserving its Sr^{2+} adsorption efficiency, demonstrating its suitability as a regenerable, recyclable adsorption material.

3.8. Adsorption Mechanism

To elucidate the mechanism of Sr^{2+} capture by KCBS, XPS spectra of KCBS and KCBS-Sr were acquired (Figure 5a). In KCBS, the characteristic peaks of K $2p_{3/2}$ and K $2p_{1/2}$ were clearly observed at approximately 292.5 eV and 295.2 eV, respectively (Figure 5b). After Sr^{2+} adsorption, these K 2p characteristic peaks disappeared in the KCBS-Sr sample, while characteristic Sr $3d_{5/2}$ and Sr $3d_{3/2}$ peaks appeared at around 133.8 eV and 135.5 eV, respectively (Figure 5c). Furthermore, the PXRD pattern reveals that after capturing Sr^{2+}, the (002) diffraction peak at a 2θ angle of 7.561° exhibits a pronounced shift towards a lower 2θ angle of 6.418° (Figure 5d), indicating an expansion of the interlayer spacing from 11.682 to 13.761 Å. This expansion is primarily attributed to the Sr^{2+} ion radius (4.12 Å) being considerably larger than that of K^+ (3.31 Å) [44], leading to interlayer spacing expansion after Sr^{2+} enters the interlayer. This behavior is similar to the Sr^{2+} ion exchange of KMS-2 [16]. In summary, combining EDS, XPS, and PXRD results confirms that KCBS achieves effective Sr^{2+} capture through ion exchange between interlayer K^+ and Sr^{2+} (Figure 5e).

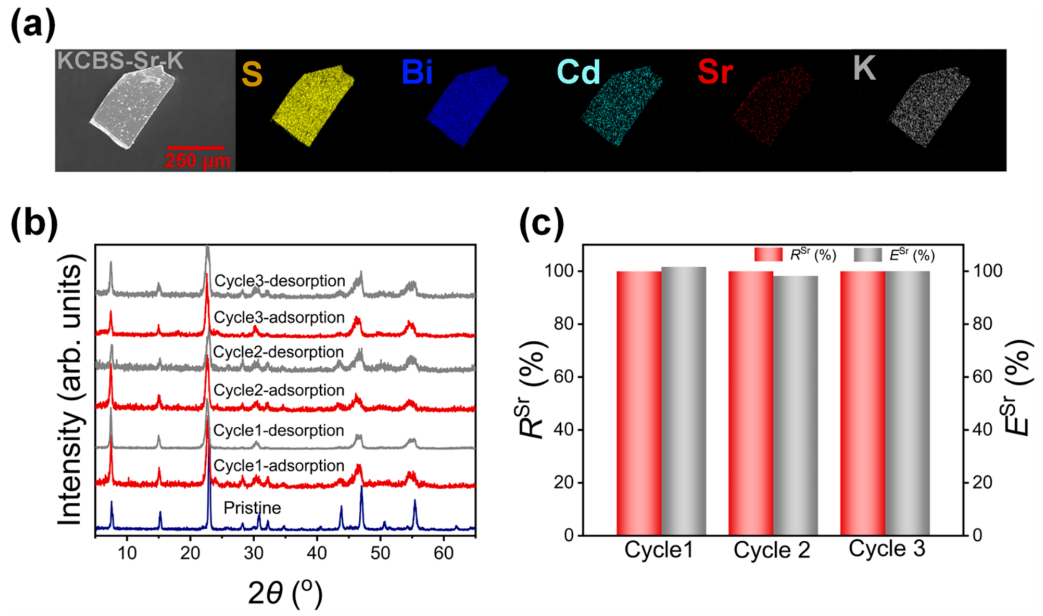


Figure 4. (**a**) SEM image and elemental distribution maps of KCBS-Sr-K. (**b**) PXRD patterns of KCBS during three adsorption–desorption cycles. (**c**) R^{Sr} (%) (red column) and E^{Sr} (%) (grey column) during three adsorption–desorption cycles.

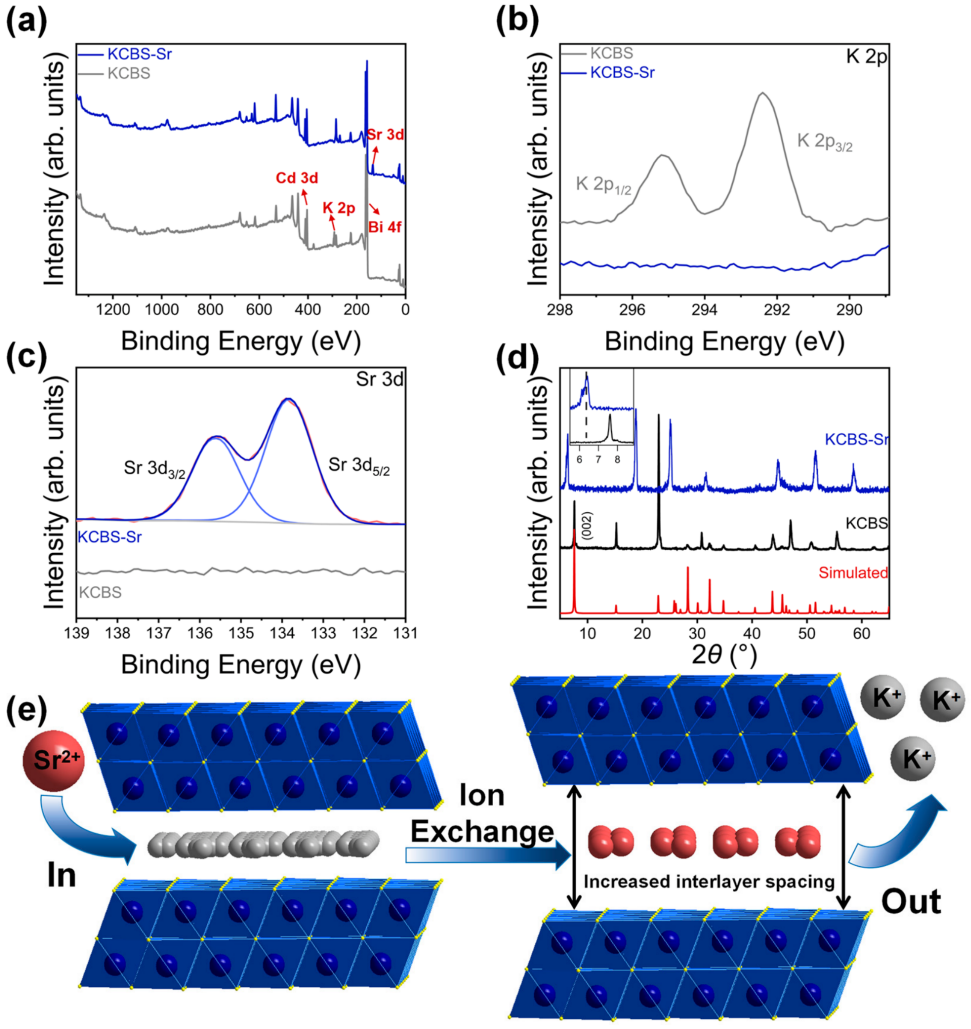


Figure 5. (**a**) Survey spectra of KCBS and KCBS-Sr. (**b**) X-ray photoelectron spectra of potassium for KCBS and KCBS-Sr. (**c**) X-ray photoelectron spectrum of strontium for KCBS-Sr. (**d**) PXRD patterns of KCBS-Sr, pristine KCBS, and simulated KCBS. (**e**) Illustration of the KCBS ion exchange of Sr^{2+}.

4. Conclusions

In this study, a metal sulfide ion exchanger, $K_{1.36}Cd_{1.12}Bi_{2.80}S_6$ (KCBS), was successfully synthesized for the efficient removal of Sr^{2+} from water environments. The structure of KCBS features the anionic layers of $[Cd_{1.12}Bi_{2.80}S_6]_n^{1.36n-}$ with K^+ ions located in the interlayer spaces. KCBS exhibits a high Sr^{2+} adsorption capacity of 77 mg·g^{-1} and rapid adsorption kinetics, achieving 95.08% Sr^{2+} removal within 30 min. It maintains outstanding stability and adsorption performance across a broad pH range (2.98–12.01), with extremely low leaching of cadmium and bismuth. Crucially, KCBS with good renewability can be reused for three adsorption–desorption cycles without structural degradation, maintaining over 99.94% removal efficiency. Mechanism studies confirm that Sr^{2+} removal primarily relies on ion exchange with interlayer K^+ ions, concurrently accompanied by significant interlayer spaces expansion due to Sr^{2+} intercalation. This study comprehensively demonstrates that KCBS represents a promising inorganic ion exchange material for Sr^{2+} capture. This finding provides significant reference for developing advanced metal sulfide ion exchange materials for radionuclide remediation. Although MSIEs presently exhibit excellent adsorption properties for Sr^{2+} at the laboratory stage, several issues remain to be addressed. For instance, synthetic methods for metal sulfides require further exploration to produce structurally novel and high-performance MSIEs. In addition, composite MSIEs with good mechanical stability and ease of handling should be further developed to meet the demands of practical applications.

Supplementary Materials: The following supporting information can be downloaded at https://www.mdpi.com/article/10.3390/separations13020071/s1. Figure S1: EDS analysis results of (a) KCBS and (b) KCBS-Sr. (c) TGA curves for KCBS and KCBS-Sr; Figure S2: SEM images of (a–c) KCBS and (d–f) KCBS-Sr at different magnifications; Figure S3: Pseudo-first-order kinetics model and pseudo-second-order kinetic model fitting curves for kinetic data of KCBS for Sr^{2+} capture; Figure S4: (a) Experimental PXRD patterns for KCBS and its corresponding samples after soaking in solutions with different pH. (b) Cd and Bi leaching percentage curves of KCBS in solutions with different pH; Figure S5: K_d (mL·g^{-1}) (column) and R (%) (dotted line plot) of KCBS for Sr^{2+}, Cs^+ and Na^+ capture in solutions with different Sr/Na/Cs molar ratios; Figure S6: K_d (mL·g^{-1}) (column) and R (%) (dotted line plot) of KCBS for Sr^{2+} and Ca^{2+} capture in solutions with different Ca/Sr molar ratios; Figure S7: PXRD patterns of KCBS samples before and after β and γ irradiations; Figure S8: (a) PXRD patterns of KCBS, KCBS-Sr, and KCBS-Sr-K. (b) EDS analysis results of KCBS-Sr-K; Table S1: Crystallographic data and structural refinements for compounds KCBS; Table S2: Selected bond lengths (Å) for KCBS; Table S3: Selected bond angles (°) for KCBS; Table S4: Fractional atomic coordinates, equivalent isotropic displacement parameters (Å^2 × 10^3), SOFs, and atomic sites for KCBS, U(eq) is defined as 1/3 of the trace of the orthogonalized U^{ij} tensor; Table S5: Experimental results of isothermal adsorption of KCBS for Sr^{2+} (V/m = 1000 mL·g^{-1} at room temperature, 12 h contact time); Table S6: Fitting parameters of the Langmuir, Freundlich, and Langmuir–Freundlich models for the isothermal adsorption of KCBS for Sr^{2+}; Table S7: Comparison of the adsorption capacities of KCBS with other reported materials for Sr^{2+}; Table S8: Experimental results on the kinetics of KCBS for Sr^{2+} (V/m = 1000 mL·g^{-1}; at room temperature); Table S9: Kinetic fitting parameters of KCBS for Sr^{2+} capture; Table S10: Thermodynamic parameters of Sr^{2+} adsorption by KCBS; Table S11: pH-dependent adsorption results of KCBS for Sr^{2+} ions removal and leaching percentages of Cd and Bi for KCBS immersed in solutions with different pH values (V/m = 1000 mL·g^{-1}, contact time 12 h at room temperature); Table S12: Adsorption results of KCBS under different Sr/Na molar ratios (V/m = 1000 mL·g^{-1}, at room temperature and 12 h contact time); Table S13: The Sr^{2+} adsorption results of KCBS under different Sr/Na/Cs molar ratios (V/m = 1000mL·g^{-1}, at room temperature and 12 h contact time); Table S14: Adsorption results of KCBS under different Sr/Mg molar ratios (V/m = 1000 mL·g^{-1}, at room temperature and 12 h contact time); Table S15: Adsorption results of KCBS under different Sr/Ca molar ratios (V/m = 1000 mL·g^{-1}, at room temperature and 12 h contact time); Table S16: Adsorption results of Sr^{2+} by KCBS under co-

existing conditions of Sr/Na/Cs/Mg/Ca (V/m = 1000 mL·g^{-1}, at room temperature and 12 h contact time); Table S17: The results on Sr^{2+} ions removal by KCBS in actual water samples contaminated with Sr^{2+} ions (V/m = 1000 mL·g^{-1}, at room temperature and 12 h contact time); Table S18: The results on Sr^{2+} ions removal by the KCBS before and after γ- and β-irradiated samples (V/m = 1000 mL·g^{-1}, at room temperature and 12 h contact time); Table S19: Results of cycling experiments.

Author Contributions: Writing—original draft preparation, L.Q.; data curation, L.Q.; visualization, L.Q.; review and editing, L.Q., Y.F., Z.W., M.F., and X.H.; project administration, M.F. All authors have read and agreed to the published version of the manuscript.

Funding: This research was funded by the National Natural Science Foundation of China (Nos. 22325605, 22576204, U21A20296, 22076185, and 22406185), the Natural Science Foundation of Fujian Province (No. 2024J08105), and the Strategic Priority Research Program of the Chinese Academy of Sciences (No. XDB1170000).

Data Availability Statement: The original contributions presented in this study are included in the article/Supplementary Materials. Further inquiries can be directed to the corresponding authors.

Conflicts of Interest: The authors declare no conflicts of interest.

References

1. Alwaeli, M.; Mannheim, V. Investigation into the Current State of Nuclear Energy and Nuclear Waste Management-A State-of-the-Art Review. *Energies* **2022**, *15*, 4275. [CrossRef]
2. McCloy, J.S.; Riley, B.J.; Wilkins, M.C.D.; Evarts, J.S.; Bussey, J.; Vienna, J.D.; Bingham, P.A.; Gregg, D.J.; Ojovan, M.; Schuller, S.; et al. International perspectives on glass waste form development for low-level and intermediate-level radioactive waste. *Mater. Today* **2024**, *80*, 594–618. [CrossRef]
3. Takao, K. How does chemistry contribute to circular economy in nuclear energy systems to make them more sustainable and ecological. *Dalton Trans.* **2023**, *52*, 9866–9881. [CrossRef]
4. Nash, K.L.; Braley, J.C. Chemistry of radioactive materials in the nuclear fuel cycle. In *Advanced Separation Techniques for Nuclear Fuel Reprocessing and Radioactive Waste Treatment*; Woodhead Publishing: Cambridge, UK, 2011; pp. 3–22. [CrossRef]
5. Selby, H.D.; Mac Innes, M.R.; Barr, D.W.; Keksis, A.L.; Meade, R.A.; Burns, C.J.; Chadwick, M.B.; Wallstrom, T.C. Fission Product Data Measured at Los Alamos for Fission Spectrum and Thermal Neutrons on ^{239}Pu, ^{235}U, ^{238}U. *Nucl. Data Sheets* **2010**, *111*, 2891–2922. [CrossRef]
6. Neis, P.; Hille, R.; Paschke, M.; Pilwat, G.; Schnabel, A.; Niess, C.; Bratzke, H. Strontium-90 for determination of time since death. *Forensic Sci. Int.* **1999**, *99*, 47–51. [CrossRef]
7. Martell, E.A. Atmospheric Aspects of Strontium-90 Fallout: Fallout evidence indicates short stratospheric holdup time for middle-latitude atomic tests. *Science* **1959**, *129*, 1197–1206. [CrossRef] [PubMed]
8. Burger, A.; Lichtscheidl, I. Strontium in the environment: Review about reactions of plants towards stable and radioactive strontium isotopes. *Sci. Total Environ.* **2019**, *653*, 1458–1512. [CrossRef] [PubMed]
9. Wang, J.C.; Jing, S.; Chen, J. Demonstration of a crown ether process for partitioning strontium from high level liquid waste (HLLW). *Radiochim. Acta* **2016**, *104*, 107–115. [CrossRef]
10. Xiao, C.L.; Hassanzadeh Fard, Z.; Sarma, D.; Song, T.B.; Xu, C.; Kanatzidis, M.G. Highly Efficient Separation of Trivalent Minor Actinides by a Layered Metal Sulfide ($KInSn_2S_6$) from Acidic Radioactive Waste. *J. Am. Chem. Soc.* **2017**, *139*, 16494–16497. [CrossRef]
11. Bikit, K.; Knezevic, J.; Mrdja, D.; Todorovic, N.; Kuzmanovic, P.; Forkapic, S.; Nikolov, J.; Bikit, I. Application of ^{90}Sr for industrial purposes and dose assessment. *Radiat. Phys. Chem.* **2021**, *179*, 109260. [CrossRef]
12. Coudert, F.X. Strontium's scarlet sparkles. *Nat. Chem.* **2015**, *7*, 940. [CrossRef]
13. Kavitha, E.; Prabhakar, S. Review and assessment on the separation of cesium and strontium from the aqueous stream. *Desal. Water Treat.* **2022**, *251*, 43–56. [CrossRef]
14. Li, W.A.; Peng, Y.C.; Ma, W.; Huang, X.Y.; Feng, M.L. Rapid and selective removal of Cs^+ and Sr^{2+} ions by two zeolite-type sulfides via ion exchange method. *Chem. Eng. J.* **2022**, *442*, 136377. [CrossRef]
15. Feng, M.L.; Sarma, D.; Gao, Y.J.; Qi, X.H.; Li, W.A.; Huang, X.Y.; Kanatzidis, M.G. Efficient Removal of UO_2^{2+}, Cs^+, and Sr^{2+} Ions by Radiation-Resistant Gallium Thioantimonates. *J. Am. Chem. Soc.* **2018**, *140*, 11133–11140. [CrossRef] [PubMed]
16. Manos, M.J.; Kanatzidis, M.G. Metal sulfide ion exchangers: Superior sorbents for the capture of toxic and nuclear waste-related metal ions. *Chem. Sci.* **2016**, *7*, 4804–4824. [CrossRef]

17. Amesh, P.; Suneesh, A.S.; Venkatesan, K.A.; Maheswari, R.U.; Vijayalakshmi, S. Preparation and ion exchange studies of cesium and strontium on sodium iron titanate. *Sep. Purif. Technol.* **2020**, *238*, 116393. [CrossRef]
18. Solbrå, S.; Allison, N.; Waite, S.; Mikhalovsky, S.V.; Bortun, A.I.; Bortun, L.N.; Clearfield, A. Cesium and strontium ion exchange on the framework titanium silicate $M_2Ti_2O_3SiO_4{\cdot}nH_2O$ (M = H, Na). *Environ. Sci. Technol.* **2001**, *35*, 626–629. [CrossRef]
19. Dyer, A.; Chow, J.K.K.; Umar, I.M. The uptake of caesium and strontium radioisotopes onto clays. *J. Mater. Chem.* **2000**, *10*, 2734–2740. [CrossRef]
20. Sinha, P.K.; Lal, K.B.; Panicker, P.K.; Krishnasamy, V. A comparative study on indigenously available synthetic zeolites for removal of strontium from solutions by ion-exchange. *Radiochim. Acta* **1996**, *73*, 157–163. [CrossRef]
21. Lan, Y.; Su, Z.; Li, X.L.; Jiang, Z.Q.; Jin, J.; Xie, J.L.; Li, S.J. Synthesis of a new microporous indium sulphide and its capabilities to the separation of strontium. *J. Radioanal. Nucl. Chem.* **2007**, *273*, 99–102. [CrossRef]
22. Tang, J.H.; Feng, M.L.; Huang, X.Y. Metal chalcogenides as ion-exchange materials for the efficient removal of key radionuclides: A review. *Fundam. Res.* **2025**, *5*, 1969–1987. [CrossRef]
23. Tang, J.H.; Sun, H.Y.; Ma, W.; Feng, M.L.; Huang, X.Y. Recent Progress in Developing Crystalline Ion Exchange Materials for the Removal of Radioactive Ions. *Chin. J. Struct. Chem.* **2020**, *39*, 2157–2171. [CrossRef]
24. Feng, M.L.; Kong, D.N.; Xie, Z.L.; Huang, X.Y. Three-Dimensional Chiral Microporous Germanium Antimony Sulfide with Ion-Exchange Properties. *Angew. Chem. Int. Ed.* **2008**, *47*, 8623–8626. [CrossRef]
25. Li, J.L.; Jin, J.C..; Zou, Y.M.; Sun, H.Y.; Zeng, X.; Huang, X.Y.; Feng, M.L.; Kanatzidis, M.G. Efficient Removal of Cs^+ and Sr^{2+} Ions by Granulous $(Me_2NH_2)_{4/3}(Me_3NH)_{2/3}Sn_3S_7{\cdot}1.25H_2O$/Polyacrylonitrile Composite. *ACS Appl. Mater. Interfaces* **2021**, *13*, 13434–13442. [CrossRef]
26. Lv, C.; Liu, L.P.; He, J.H.; Yang, L.; Liu, J.T.; Xia, C.Q.; Huang, X.Y.; Feng, M.L. Efficient uranium adsorption of low-cost and eco-friendly MQ_2-collagen fibers (M = Mo, W.; Q = S, Se) composite materials prepared by co-ball milling. *Natl. Sci. Open* **2025**, *4*, 20240029. [CrossRef]
27. Mertz, J.L.; Fard, Z.H.; Malliakas, C.D.; Manos, M.J.; Kanatzidis, M.G. Selective Removal of Cs^+, Sr^{2+}, and Ni^{2+} by $K_{2x}Mg_xSn_{3-x}S_6$ (x = 0.5-1) (KMS-2) Relevant to Nuclear Waste Remediation. *Chem. Mater.* **2013**, *25*, 2116–2127. [CrossRef]
28. Sarma, D.; Islam, S.M.; Subrahmanyam, K.S.; Kanatzidis, M.G. Efficient and selective heavy metal sequestration from water by using layered sulfide $K_{2x}Sn_{4-x}S_{8-x}$ (x = 0.65-1; KTS-3). *J. Mater. Chem. A* **2016**, *4*, 16597–16605. [CrossRef]
29. Zhang, Z.G.; Gu, P.; Zhang, M.D.; Yan, S.; Dong, L.H.; Zhang, G.H. Synthesis of a robust layered metal sulfide for rapid and effective removal of Sr^{2+} from aqueous solutions. *Chem. Eng. J.* **2019**, *372*, 1205–1215. [CrossRef]
30. Guo, J.N.; Wang, Z.X.; Zhang, G.H.; Liu, S.R.; Dong, L.H.; Gu, P.; Hou, L.A. Rapid and effective removal of strontium ions from aqueous solutions by a novel layered metal sulfide NaTS-2. *J. Radioanal. Nucl. Chem.* **2023**, *332*, 2367–2378. [CrossRef]
31. Qi, X.H.; Du, K.Z.; Feng, M.L.; Li, J.R.; Du, C.F.; Zhang, B.; Huang, X.Y. A two-dimensionally microporous thiostannate with superior Cs^+ and Sr^{2+} ion-exchange property. *J. Mater. Chem. A* **2015**, *3*, 5665–5673. [CrossRef]
32. Li, W.A.; Li, J.R.; Zhang, B.; Sun, H.Y.; Jin, J.C.; Huang, X.Y.; Feng, M.L. Layered Thiostannates with Distinct Arrangements of Mixed Cations for the Selective Capture of Cs^+, Sr^{2+}, and Eu^{3+} Ions. *ACS Appl. Mater. Interfaces* **2021**, *13*, 10191–10201. [CrossRef]
33. Ren, Y.W.; Luo, J.H.; Chen, Z.H.; Liu, S.Z.; Guo, X.P.; Chen, G.Y.; Feng, M.L.; Huang, X.Y. The efficient removal of Sr^{2+} using two thiostannates via ion exchange. *Dalton Trans.* **2025**, *54*, 15055–15061. [CrossRef]
34. Wang, K.Y.; Sun, M.; Ding, D.; Liu, H.W.; Cheng, L.; Wang, C. Di-lacunary $[In_6S_{15}]^{12-}$ cluster: The building block of a highly negatively charged framework for superior Sr^{2+} adsorption capacities. *Chem. Commun.* **2020**, *56*, 3409–3412. [CrossRef] [PubMed]
35. Wei, C.; Jia, S.Q.; Zhao, Y.Y.; Liu, J.T.; Sun, H.Y.; Feng, M.L.; Huang, X.Y. Efficient capture of Cs^+ and Sr^{2+} by layered thioniobates and thiotantalate and insight into the structure-property relationship. *Sci. China Chem.* **2025**, *68*, 4856–4866. [CrossRef]
36. Zhao, J.; Islam, S.M.; Kontsevoi, O.Y.; Tan, G.J.; Stoumpos, C.C.; Chen, H.J.; Li, R.K.; Kanatzidis, M.G. The Two-Dimensional $A_xCd_xBi_{1-x}Q_6$ (A = K, Rb, Cs; Q = S, Se): Direct Bandgap Semiconductors and Ion-Exchange Materials. *J. Am. Chem. Soc.* **2017**, *139*, 6978–6987. [CrossRef] [PubMed]
37. Lu, Y.J.; Ibers, J.A. Synthesis and characterization of the new quaternary two-dimensional materials KCu_2NbQ_4 (Q = Se, S). *J. Solid State Chem.* **1991**, *94*, 381–385. [CrossRef]
38. Wei, C.; Jia, S.Q.; Zhao, Y.Y.; Liu, J.T.; Sun, H.Y.; Feng, M.L.; Huang, X.Y. A Two-Dimensional Thiotitanate Ion Exchanger with High Cs^+ Removal Performance. *Separations* **2025**, *12*, 104. [CrossRef]
39. Duong, D.D. *Adsorption Analysis: Equilibria and Kinetics*; World Scientific Publishing Co. Pte. Ltd.: Singapore, 1998; 916p. [CrossRef]
40. Zhang, M.D.; Gu, P.; Yan, S.; Dong, L.H.; Zhang, G.H. Na/Zn/Sn/S (NaZTS): Quaternary metal sulfide nanosheets for efficient adsorption of radioactive strontium ions. *Chem. Eng. J.* **2020**, *379*, 122227. [CrossRef]
41. Chen, Y.; Wang, Z.X.; Liu, S.R.; Zhang, G.H.; Dong, L.H.; Gu, P.; Hou, L.A. Layered metal sulfide NMTS for rapid removal of radioactive strontium ions from aqueous solution. *Sep. Purif. Technol.* **2023**, *310*, 122887. [CrossRef]
42. Zhang, L.; Wei, J.Y.; Zhao, X.; Li, F.Z.; Jiang, F.; Zhang, M.; Cheng, X.Z. Competitive adsorption of strontium and cobalt onto tin antimonate. *Chem. Eng. J.* **2016**, *285*, 679–689. [CrossRef]

43. Paark, Y.; Lee, Y.C.; Shin, W.S.; Choi, S.J. Removal of cobalt, strontium and cesium from radioactive laundry wastewater by ammonium molybdophosphate-polyacrylonitrile (AMP-PAN). *Chem. Eng. J.* **2010**, *162*, 685–695. [CrossRef]
44. Nightingale, E.R. Phenomenological Theory of Ion Solvation—Effective Radii of Hydrated Ions. *J. Phys. Chem.* **1959**, *63*, 1381–1387. [CrossRef]

Disclaimer/Publisher's Note: The statements, opinions and data contained in all publications are solely those of the individual author(s) and contributor(s) and not of MDPI and/or the editor(s). MDPI and/or the editor(s) disclaim responsibility for any injury to people or property resulting from any ideas, methods, instructions or products referred to in the content.